Passivity-based Force-Motion Control of Humanoids with Contact and Posture Constraints

Gerardo Jarquín Gustavo Arechavaleta Ernesto Olguín-Díaz Vicente Parra-Vega
Robótica y Manufactura Avanzada, Cinvestav-IPN, Unidad Saltillo
{gerardo.jarquin,garechav,ernesto.olguin,vicente.parra}@cinvestav.edu.mx

***Resumen*— We propose a passivity-based model-free second order sliding mode control law to track desired humanoid posture and contact force trajectories. Desired posture trajectories are generated in closed-loop by means of priority-based inverse kinematics. At each instant of time, the resulting humanoid posture is projected on the tangent subspace of the contact manifolds. Overall, the proposed force-motion control scheme accounts for the constrained dynamics in closed-loop of underactuated and highly redundant mechanical systems such as humanoids. Exponential convergence of posture and contact force tracking errors is guaranteed. We successfully verified in simulation the robustness of the controller with a realistic dynamic model of HRP-2.**

I. Introduction

In humanoid robotics, a lot of research efforts have been conducted to control the mobility of these anthropomorphic mechanisms. It is worth commenting on the Resolved Motion Rate Control schemes commonly carried out for task prioritization purposes (Liégeois, 1977; Nakamura *et al.*, 1987; Siciliano and Slotine, 1991; Gienger *et al.*, 2005). Normally, an array of operational tasks consisting of carefully designed arrangements of constraints is used. Sophisticated least-squares minimization strategies have also been developed in order to guarantee real-time solutions at kinematic level (Kanoun, 2011). However, the generation of dynamic humanoid motions needs to handle multicontact interactions while keeping dynamic balance (Hyon and Cheng, 2006; Sentis *et al.*, 2010; Saab *et al.*, 2011).

Probably, the most popular family of force-motion controllers are based on (Raibert and Craig, 1981) and (Khatib, 1987) to construct a control law. In general, two manifolds are used: *a)* the cotangent subspace defined by contact constraints where operational forces belong; and *b)* its tangent subspace of unconstrained joint velocities. Although priority-based inverse dynamics effectively solves the problem, it demands extensive computation. This is mainly due to the change of generalized joint coordinates to the operational counterpart (Khatib, 1987).

Contrary to the whole-body passivity-based controller presented in (Hyon and Cheng, 2006), the present work takes advantage of efficient priority-based inverse kinematics (PIK) within a dynamic controller (see Figure 1). The solution shapes the extended errors used to preserve passivity and the energetic performance of the humanoid robot in closed-loop. In contrast to our previous work on cooperative redundant arms (Arechavaleta *et al.*, 2010), here, the control scheme is extended to the case of non-inertial tree-like kinematic mechanisms subject to balancing. The salient feature of the proposed scheme is that we construct the control law by purely kinematic operators regardless the regressor. Moreover, it ensures exponential convergence of joint position, velocity and force errors in tracking regime. The remaining of this paper is organized as follows. In Section II we derive the necessary operators for modeling constrained humanoid motions. Then, in Section III we define operational tasks within the PIK framework. Section IV presents the force-motion control scheme. In Section V representative simulation scenarios illustrate the effectiveness of the proposed control framework. Finally, we provide in Section VI some concluding remarks.

II. Humanoid dynamics

Humanoid robots are multi body systems with non-inertial kinematic tree-like structure. The base frame is commonly attached to the pelvis and encodes the underactuated degrees of freedom (dof). The arms, legs and head can be seen as kinematic branches attached to the non-inertial base. Lets define the configuration of the humanoid robot as

$$\boldsymbol{q} \triangleq \begin{pmatrix} \boldsymbol{q}_b \\ \boldsymbol{q}_e \end{pmatrix} \in \mathcal{CS}$$

where $\boldsymbol{q}_b \in \mathbb{R}^3 \times SO(3)$ represents the base coordinates, $\boldsymbol{q}_e$ stands for the humanoid kinematic chains and $n = \dim(\mathcal{CS})$. The equations of motion of a humanoid robot can be written as:

$$H(\boldsymbol{q})\ddot{\boldsymbol{q}} + \boldsymbol{h}(\boldsymbol{q}, \dot{\boldsymbol{q}}) = S^T\boldsymbol{\tau} + \boldsymbol{\tau}_c \tag{1}$$

where $H(\boldsymbol{q}) \in \mathbb{R}^{n\times n}$ is the symmetric, positive definite inertial matrix, $\boldsymbol{h}(\boldsymbol{q}, \dot{\boldsymbol{q}}) = C(\boldsymbol{q}, \dot{\boldsymbol{q}})\dot{\boldsymbol{q}} + D(\cdot)\dot{\boldsymbol{q}} + \boldsymbol{g}(\boldsymbol{q})$ contains the Coriolis vector $C(\boldsymbol{q}, \dot{\boldsymbol{q}})\dot{\boldsymbol{q}}$, the damping vector $D(\cdot)\dot{\boldsymbol{q}}$ expresses the inner dissipative energy of the system and the gravity vector. The generalized external and contact forces are $\boldsymbol{\tau}$ and $\boldsymbol{\tau}_c$, respectively. It is important to note that $S = [0\ I]$ selects the actuated joints and $\ddot{\boldsymbol{q}}$ should be expressed as

$$\ddot{\boldsymbol{q}} \triangleq \begin{pmatrix} \dot{\boldsymbol{\nu}}_r \\ \ddot{\boldsymbol{q}}_e \end{pmatrix} \in \mathbb{R}^n$$

where $\boldsymbol{\nu}_r = (\boldsymbol{v}^T\ \boldsymbol{\omega}^T)^T \in \mathbb{R}^6$ is the *twist* of the non-inertial base, $(\boldsymbol{v}, \boldsymbol{\omega}) \in \mathbb{R}^3$ are the linear and angular

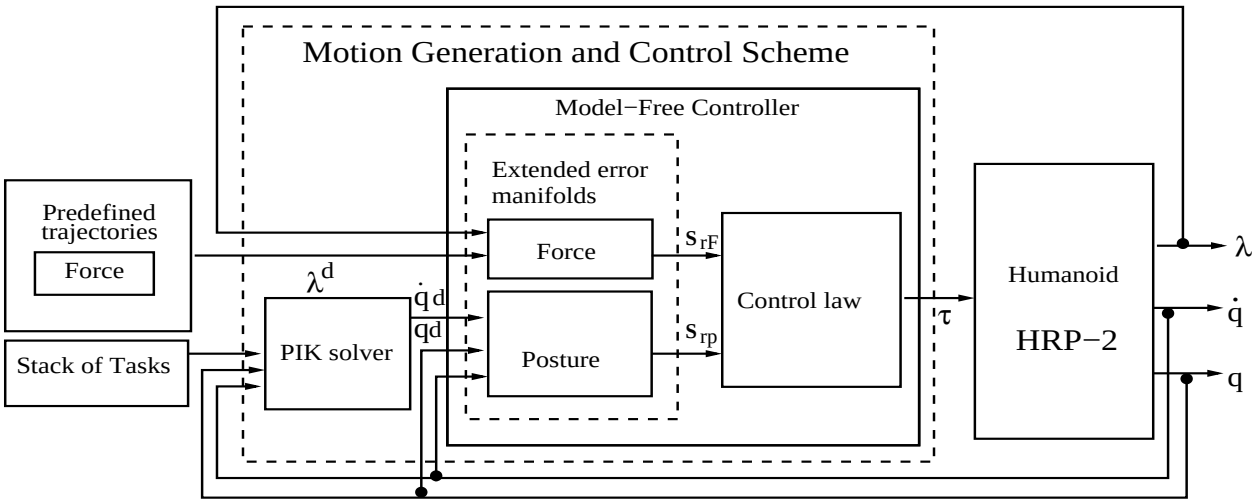

Figura 1. Motion generation and control scheme. The motion generation is based on PIK and it gives the instantaneous joint and velocities coordinates to be tracked by a passivity-based force-motion controller.

velocities respectively. Then, let us define the following linear operator that maps $\dot{\boldsymbol{q}}_b \mapsto \boldsymbol{\nu}_r$:

$$J_x(\boldsymbol{\vartheta}) \triangleq \begin{bmatrix} I & 0 \\ 0 & J_\vartheta(\boldsymbol{\vartheta}) \end{bmatrix} \tag{2}$$

where $I \in \mathbb{R}^{3\times 3}$ is the identity matrix and $J_\vartheta(\boldsymbol{\vartheta}) \in \mathbb{R}^{3\times l}$ is uniquely defined as

$$J_\vartheta(\boldsymbol{\vartheta}) \triangleq \frac{1}{2}\left[[\boldsymbol{r}_1\times]\frac{\partial \boldsymbol{r}_1}{\partial \boldsymbol{\vartheta}} + [\boldsymbol{r}_2\times]\frac{\partial \boldsymbol{r}_2}{\partial \boldsymbol{\vartheta}} + [\boldsymbol{r}_3\times]\frac{\partial \boldsymbol{r}_3}{\partial \boldsymbol{\vartheta}}\right] \tag{3}$$

knowing that $R(\boldsymbol{\vartheta}) = [\boldsymbol{r}_1, \boldsymbol{r}_2, \boldsymbol{r}_3] \in \mathcal{SO}(3)$ and $\boldsymbol{\vartheta} \in \mathbb{R}^l$, $l \geq 3$.

A. Contact forces

Lets recall the power transmission principle $P = \boldsymbol{\nu}^T \boldsymbol{F}$ where $\boldsymbol{\nu}$ is the *twist* at an operational point belonging to the humanoid kinematic chains and $\boldsymbol{F} = (\boldsymbol{f}^T \ \boldsymbol{n}^T)^T \in \mathbb{R}^6$ is the *wrench* (i.e. force and torque) acting exactly at the same operational point. Therefore, the generalized contact force given by *external wrenches* can be expressed as:

$$\boldsymbol{\tau}_c = J_c^T(\boldsymbol{q})\boldsymbol{F}_c \tag{4}$$

where the contact Jacobian and force have the structure:

$$\begin{aligned} J_c^T(\boldsymbol{q}) &\triangleq \left[J_{c_1}^T(\boldsymbol{q}), ..., J_{c_r}^T(\boldsymbol{q})\right] \in \mathbb{R}^{6r\times n} \\ \boldsymbol{F}_c &\triangleq (\boldsymbol{F}_{c_1}^T, ..., \boldsymbol{F}_{c_r}^T)^T \in \mathbb{R}^{6r} \end{aligned}$$

such that the following expression holds:

$$\boldsymbol{\nu}_c = J_c(\boldsymbol{q})\dot{\boldsymbol{q}} \tag{5}$$

where $\boldsymbol{\nu}_c \triangleq (\boldsymbol{\nu}_{c_1}^T, ..., \boldsymbol{\nu}_{c_r}^T)^T \in \mathbb{R}^{6r}$ is the contact velocity. Each Jacobian $J_{c_i}(\boldsymbol{q})$ is computed as in (Dubowsky and Papadopoulos, 1993) to map $\dot{\boldsymbol{q}} \to \boldsymbol{\nu}_{c_i}$.

B. Constrained dynamics

The humanoid constrained dynamics with multiple contact points is then formulated as

$$H(\boldsymbol{q})\ddot{\boldsymbol{q}} + \boldsymbol{h}(\boldsymbol{q}, \dot{\boldsymbol{q}}) = \boldsymbol{\tau} + J_c^T(\boldsymbol{q})\boldsymbol{F}_c \tag{6}$$

$$\text{s.t.} \quad J_c(\boldsymbol{q})\dot{\boldsymbol{q}} = \boldsymbol{\nu}_c \tag{7}$$

When $\boldsymbol{F}_c$ is directly measured from sensors, it can be introduced in the nonlinear term $\boldsymbol{h}$. However, for simulation purposes (6)-(7) must be solved. Thus, by computing the second derivative of (7) w.r.t. time, we rewrite the whole system as

$$\begin{bmatrix} H & -J_c^T \\ -J_c & 0 \end{bmatrix}\begin{pmatrix} \ddot{\boldsymbol{q}} \\ \boldsymbol{F}_c \end{pmatrix} = \begin{pmatrix} \boldsymbol{\tau} - \boldsymbol{h} \\ \dot{J}_c\dot{\boldsymbol{q}} - \dot{\boldsymbol{\nu}}_c \end{pmatrix} \tag{8}$$

III. Operational tasks for motion generation

Operational tasks are composed by linear equality and inequality constraints. The former allows to reach a fixed target and to maintain contacts while inequalities serve to avoid collisions and joint limits but also to maintain the projection of the humanoid center of mass (CoM) within the supporting polygon defined on the floor[1].

A. Posture tasks

To compute humanoid postures, we define equality tasks of the form

$$\boldsymbol{e}(\boldsymbol{q}) = \boldsymbol{x}^d - f(\boldsymbol{q}) \to 0 \tag{9}$$

where the desired operational target is $\boldsymbol{x}^d$ and $f(\boldsymbol{q})$ permits to evaluate the current state of the task in terms of the robot configuration. The exponential convergence of $\boldsymbol{e}(\boldsymbol{q})$ can be achieved by $\dot{\boldsymbol{e}}(\boldsymbol{q}) = -\alpha\boldsymbol{e}(\boldsymbol{q})$. The task Jacobian is obtained by differentiating (9) w.r.t. time such that

$$J(\boldsymbol{q})\dot{\boldsymbol{q}} = -\alpha\boldsymbol{e}(\boldsymbol{q}) \tag{10}$$

[1]Note that the humanoid CoM can be obtained from a ZMP reference.

where $J(\boldsymbol{q}) \in \mathbb{R}^{m\times n}$ and m is the dimension of the task space. When $m < n$, the null-space of $J(\boldsymbol{q})$ associated to $\boldsymbol{e}(\boldsymbol{q})$ is commonly used to solve additional secondary tasks without altering the primary task. In this case, the inverse mapping between $\dot{\boldsymbol{e}}$ and $\dot{\boldsymbol{q}}$ is obtained by applying the Moore-Penrose inverse as

$$\dot{\boldsymbol{q}} = J^{+}(\boldsymbol{q})\dot{\boldsymbol{e}} + Q(\boldsymbol{q})\boldsymbol{z}_{null} \tag{11}$$

where $J^{+}(\boldsymbol{q}) = J^{T}(\boldsymbol{q})\left(J(\boldsymbol{q})J^{T}(\boldsymbol{q})\right)^{-1}$. The orthogonal projection of $J(\boldsymbol{q})$ is defined as

$$Q(\boldsymbol{q}) \triangleq I_n - J^{+}(\boldsymbol{q})J(\boldsymbol{q}) \tag{12}$$

which spans the $n-m$-dimensional null-space of $J(\boldsymbol{q})$ and $\boldsymbol{z}_{null}$ is an arbitrary vector. In general, a hierarchical structure $\{\boldsymbol{e}_1(\boldsymbol{q})\ \boldsymbol{e}_2(\boldsymbol{q})\ \ldots\ \boldsymbol{e}_p(\boldsymbol{q})\}$ can be defined where p represents the task with last priority. This means that it is possible to simultaneously solve as many operational tasks as degrees of freedom (dof) are available.

B. Contact tasks

Contacts between the robot and the environment can be considered as holonomic constraints of the form

$$\varphi(f(\boldsymbol{q})) = 0 \tag{13}$$

where $\boldsymbol{x} = f(\boldsymbol{q})$ is the end-effector pose and $\varphi(\cdot) \in \mathbb{R}^{r}$ represents the geometry of smooth surfaces in the environment. By differentiating (13) w.r.t. time, the contact task Jacobian appears

$$J_{\varphi}(\boldsymbol{q})\dot{\boldsymbol{q}} = 0$$

where $J_{\varphi}(\boldsymbol{q}) = J_{\varphi_x}(\boldsymbol{x})J(\boldsymbol{q})$ is composed by the constraint Jacobian $J_{\varphi_x}(\boldsymbol{x}) \in \mathbb{R}^{r\times 6}$ and $J(\boldsymbol{q}) \in \mathbb{R}^{6\times n}$ is the Jacobian at the contact point. Clearly, $rank\{J_{\varphi}(\boldsymbol{q})\} = r$, for $r < n$ contact points. Then, it is possible to construct an orthogonal projection of $J_{\varphi}(\boldsymbol{q})$ similar to (12) such that $rank\{Q_{\varphi}(\boldsymbol{q})\} = n - r$. This allows to project secondary posture tasks onto the tangent subspace of unconstrained joint velocities defined by the null space of $J_{\varphi}(\boldsymbol{q})$.

C. Kinematic motion generation

The following recursion reported in (Siciliano and Slotine, 1991; Baerlocher and Boulic, 2004) solves (10)-(11) at priority level i:

$$\begin{array}{l}\dot{\boldsymbol{q}}_1 = J_1(\boldsymbol{q})^{+}\dot{\boldsymbol{e}}_1 \ \text{ and} \\ \dot{\boldsymbol{q}}_i = \dot{\boldsymbol{q}}_{i-1} + (J_i(\boldsymbol{q})Q_{i-1}(\boldsymbol{q}))^{+}(\dot{\boldsymbol{e}}_i - J_i(\boldsymbol{q})\dot{\boldsymbol{q}}_{i-1})\end{array} \tag{14}$$

Using the quadratic programing (QP) formulation suggested in (Kanoun *et al.*, 2011), it is possible to cope with mixed linear systems. In this case, the QP at priority i is expressed as

$$\begin{array}{ll}\min\limits_{\dot{\boldsymbol{q}}_i\in\mathbb{R}^n, \boldsymbol{w}\in\mathbb{R}^m} & \frac{1}{2}\parallel \boldsymbol{w}_i \parallel^2 \\ \text{s.t.} & \dot{\boldsymbol{e}}_i^{l}(\boldsymbol{q}) \le J_i(\boldsymbol{q})\dot{\boldsymbol{q}}_i - \boldsymbol{w}_i \le \dot{\boldsymbol{e}}_i^{u}(\boldsymbol{q}) \\ & \bar{\dot{\boldsymbol{e}}}_{i-1}^{l}(\boldsymbol{q}) \le \bar{J}_{i-1}(\boldsymbol{q})\dot{\boldsymbol{q}}_i \le \bar{\dot{\boldsymbol{e}}}_{i-1}^{u}(\boldsymbol{q})\end{array} \tag{15}$$

where the superscripts l and u stands for the lower and upper limits, respectively. Moreover

$$\bar{J}_i(\boldsymbol{q}) = \begin{bmatrix}\bar{J}_{i-1}(\boldsymbol{q}) \\ J_i(\boldsymbol{q})\end{bmatrix},\quad \bar{\dot{\boldsymbol{e}}}_i(\boldsymbol{q}) = \begin{bmatrix}\bar{\dot{\boldsymbol{e}}}_{i-1}(\boldsymbol{q}) \\ \dot{\boldsymbol{e}}_i(\boldsymbol{q}) + \boldsymbol{w}_i\end{bmatrix}$$

forms a non-empty convex polytope that maintains the solution of upper tasks. The outcome of (15), for $i = 1\ldots p$, represents the instantaneous posture reference $\dot{\boldsymbol{q}}^{d}$. At this stage, the idempotent property of $Q_{\varphi}(\boldsymbol{q})$ can be used:

$$\dot{\boldsymbol{q}}^{d} \triangleq Q_{\varphi}(\boldsymbol{q})\dot{\boldsymbol{q}}^{d} \tag{16}$$

This allows to unify the hierarchy of operational tasks by projecting the solution of the finite set of posture tasks onto the null space of the contact task Jacobian $J_{\varphi}(\boldsymbol{q})$.

IV. Force-motion control scheme

The objective of the proposed control scheme is to ensure the robust behavior of a set of prioritized posture and contact tasks for a humanoid robot. Fig. 1 illustrates the main components as well as how they are connected. The inputs are the desired profiles of operational forces (contact tasks), the initial configuration of the robot and an ordered array of posture tasks with priorities. The whole-body motion is generated by means of the PIK solver. Simultaneously, the controller guarantees the tracking of force, generalized coordinate and velocity references, $\Delta\lambda = \lambda - \lambda^{d}$, $\Delta\boldsymbol{q} = \boldsymbol{q} - \boldsymbol{q}^{d}$ and $\Delta\dot{\boldsymbol{q}} = \dot{\boldsymbol{q}} - \dot{\boldsymbol{q}}^{d}$ respectively, according to two error manifolds (i.e. operational force and posture).

A. Lagrangian mapping and linear parametrization

From the constrained Lagrangian function commonly defined as $\mathcal{L} = K - U + \varphi^{T}(\boldsymbol{x})\boldsymbol{\lambda}$ together with (2), we express the *contact wrench* in (4) as

$$\boldsymbol{F}_c = J_x^{-T}(\boldsymbol{x})J_{\varphi_x}^{T}(\boldsymbol{x})\boldsymbol{\lambda} \tag{17}$$

By applying the appropriate mapping $\boldsymbol{\nu}_r \mapsto \dot{\boldsymbol{q}}_b$ through the inverse of (2), it is straightforward to verify passivity for the corresponding open-loop Lagrangian system. We then write the equivalent Lagrangian system in terms of the following linear parametrization

$$H(\boldsymbol{q})\ddot{\boldsymbol{q}} + \boldsymbol{h}(\boldsymbol{q},\dot{\boldsymbol{q}}) = Y(\boldsymbol{q},\dot{\boldsymbol{q}},\ddot{\boldsymbol{q}})\boldsymbol{\Theta} \tag{18}$$

where the regressor $Y(\boldsymbol{q},\dot{\boldsymbol{q}},\ddot{\boldsymbol{q}}) \in \mathbb{R}^{n\times l}$ is composed by known nonlinear functions and $\boldsymbol{\Theta} \in \mathbb{R}^{l}$ includes the l unknown but constant dynamic parameters. Notice that in (18) the generalized velocity vector is written as $\dot{\boldsymbol{q}} \triangleq \begin{pmatrix}\dot{\boldsymbol{q}}_b^{T} & \dot{\boldsymbol{q}}_e^{T}\end{pmatrix}^{T} \in \mathbb{R}^{n}$. From (18) and by defining $Y_r(\boldsymbol{q},\dot{\boldsymbol{q}},\dot{\boldsymbol{q}}_r,\ddot{\boldsymbol{q}}_r)$, where $\dot{\boldsymbol{q}}_r$ represents a nominal reference, the open-loop error system is constructed

$$\begin{array}{rcl}H(\boldsymbol{q})\dot{\boldsymbol{s}} + [C(\boldsymbol{q},\dot{\boldsymbol{q}}) + D(\cdot)]\,\boldsymbol{s} & = & \boldsymbol{\tau} + J_{\varphi}^{T}(\boldsymbol{q})\boldsymbol{\lambda} \\ & & -Y_r(\cdot)\boldsymbol{\Theta}\end{array} \tag{19}$$

where $\boldsymbol{s} \triangleq \dot{\boldsymbol{q}} - \dot{\boldsymbol{q}}_r$ is called the extended error.

B. Orthogonal nominal references

Lets consider

$$\begin{aligned}\dot{\boldsymbol{q}}_r &= Q_\varphi \left(\dot{\boldsymbol{q}}^d - \alpha \Delta \boldsymbol{q} + \boldsymbol{s}_{dp} - k_{ip} \int \mathrm{sgn}(\boldsymbol{s}_{qp}) dt \right) \\ &\quad + J_\varphi^+ \beta \boldsymbol{s}_{rF} \end{aligned} \tag{20}$$

where β, α and k_{ip} are positive constant gains. Consequently, the structure of the extended error variable is given by

$$\boldsymbol{s} = Q_\varphi \boldsymbol{s}_{rp} - J_\varphi^+ \beta \boldsymbol{s}_{rF} \tag{21}$$

where the joint (posture) error manifold is

$$\begin{aligned} \boldsymbol{s}_p &= \Delta \dot{\boldsymbol{q}} + \alpha \Delta \boldsymbol{q} && \text{(22a)} \\ \boldsymbol{s}_{dp} &= \boldsymbol{s}_p(t_0) e^{-\beta_p t} && \text{(22b)} \\ \boldsymbol{s}_{qp} &= \boldsymbol{s}_p - \boldsymbol{s}_{dp} && \text{(22c)} \\ \boldsymbol{s}_{rp} &= \boldsymbol{s}_{qp} + k_{ip} \int \mathrm{sgn}(\boldsymbol{s}_{qp}) dt && \text{(22d)} \end{aligned}$$

and the force (contact) error manifold is

$$\begin{aligned} \boldsymbol{s}_F &= \int \Delta \lambda dt && \text{(23a)} \\ \boldsymbol{s}_{dF} &= \boldsymbol{s}_F(t_0) e^{-\beta_F t} && \text{(23b)} \\ \boldsymbol{s}_{qF} &= \boldsymbol{s}_F - \boldsymbol{s}_{dF} && \text{(23c)} \\ \boldsymbol{s}_{rF} &= \boldsymbol{s}_{qF} + k_{iF} \int \mathrm{sgn}(\boldsymbol{s}_{qF}) dt && \text{(23d)} \end{aligned}$$

where, β_p, β_F, k_{iF} are positive constant gains and $sgn(\cdot)$ stands for the signum function.

C. The control law

The structure of the control law is

$$\boldsymbol{\tau} = -K_d \boldsymbol{s} + J_\varphi^T \left(-\lambda^d + \dot{\boldsymbol{s}}_{dF} + k_{iF} \tanh(\mu \boldsymbol{s}_{qF}) + \eta \boldsymbol{s}_{rF} \right) \tag{24}$$

where $K_d \in \mathbb{R}^{n \times n}$, μ and η are positive constant gains and $\tanh(\cdot)$ is the hyperbolic tangent function. Then, by considering (19) and (24) the closed-loop system becomes

$$\begin{aligned} H(\boldsymbol{q}) \dot{\boldsymbol{s}} + \left[C(\boldsymbol{q}, \dot{\boldsymbol{q}}) + D(\cdot) + K_d \right] \boldsymbol{s} &= \boldsymbol{\tau}_u + J_\varphi^T \boldsymbol{Z}_F \\ &\quad - Y_r(\cdot) \boldsymbol{\Theta} \end{aligned} \tag{25}$$

where

$$\boldsymbol{Z}_F = \eta \boldsymbol{s}_{rF} + \dot{\boldsymbol{s}}_{rF} - \mathrm{sgn}(\boldsymbol{s}_{qF}) + k_{iF} \tanh(\mu \boldsymbol{s}_{qF}) \tag{26}$$

and $\boldsymbol{\tau}_u$ is a virtual vector of generalized forces useful for the passivity analysis of (25) where $\boldsymbol{\tau}_u$ is the input and $\boldsymbol{s}$ the output.

The stability proof relies on Lyapunov and second order sliding mode arguments as follows. Consider the following Lyapunov function

$$V = \frac{1}{2} \left(\boldsymbol{s}^T H(\boldsymbol{q}) \boldsymbol{s} + \beta \boldsymbol{s}_{rF}^T \boldsymbol{s}_{rF} \right) \tag{27}$$

By using the skew-symmetric property of Coriolis matrix, i.e. $\boldsymbol{\xi}(\dot{H}(\dot{\boldsymbol{q}}) - C(\dot{\boldsymbol{q}}, \boldsymbol{q}))\boldsymbol{\xi} = 0 \;\; \forall \boldsymbol{\xi} \neq 0$, the time derivative of (27) is obtained

$$\begin{aligned} \dot{V} &= -\boldsymbol{s}^T (D(\cdot) + K_d) \boldsymbol{s} - \beta \eta \boldsymbol{s}_{rF}^T \boldsymbol{s}_{rF} - \boldsymbol{s}^T Y_r(\cdot) \boldsymbol{\Theta} \\ &\quad + \boldsymbol{s}^T K_{iF} J_\varphi^T \left(\tanh(\mu \boldsymbol{s}_{qF}) - \mathrm{sgn}(\boldsymbol{s}_{qF}) \right) \end{aligned} \tag{28}$$

Notice that the boundedness of $Y_r(\cdot)\boldsymbol{\Theta}$, J_φ, Q_φ and the tangent and sign functions yields to

$$\dot{V} \leq -\boldsymbol{s}^T (D(\cdot) + K_d) \boldsymbol{s} - \beta \eta \boldsymbol{s}_{rF}^T \boldsymbol{s}_{rF} + \| \boldsymbol{s} \| \| \delta \| \tag{29}$$

According to the Lyapunov analysis, large enough values of K_d, β and η imply the asymptotic local convergence of $\boldsymbol{s}$ to a region around the origin bounded by δ. This local stability result of $\boldsymbol{s}$ ensures the boundedness of $\boldsymbol{s}_{rp}$ and $\boldsymbol{s}_{rF}$ in the $\| \cdot \|_\infty$ sense, such that $\| \dot{\boldsymbol{s}}_{rj} \|_\infty < \delta_j, \; \forall \, j = \{F, \, p\}$.

Now, the sliding mode condition (Utkin, 1992) is verified as follows

$$\begin{aligned} \boldsymbol{s}_{qj}^T \dot{\boldsymbol{s}}_{qj} &= -k_{ij} \boldsymbol{s}_{qj}^T \mathrm{sgn}(\boldsymbol{s}_{qj}) + \boldsymbol{s}_{qj}^T \dot{\boldsymbol{s}}_{rj} \\ &\leq -k_{ij} \| \boldsymbol{s}_{qj} \| + \| \boldsymbol{s}_{qj} \| \| \dot{\boldsymbol{s}}_{rj} \| \\ &\leq (\delta_j - k_{ij}) \| \boldsymbol{s}_{qj} \| \end{aligned}$$

Then for $\delta_j < k_{ij}$ a sliding mode on $\boldsymbol{s}_{qj} = 0$ is established at time $t \leq \| \boldsymbol{s}_{qj}(t_0) \| / (\delta_j - k_{ij})$. Therefore, according with (22) and (23) $\boldsymbol{s}_{qj}(t_0) = 0$ and, consequently, there exists a sliding mode for all time. This result implies that $\boldsymbol{s}_{rj} \to 0$ locally, which leads to the exponential convergence of the tracking errors, i.e. $\Delta \lambda \to 0$, $\Delta \boldsymbol{q} \to 0$ and $\Delta \dot{\boldsymbol{q}} \to 0$.

V. Simulations

In order to compute the generalized acceleration and contact forces in simulation we applied spatial algebra based on extended rotation and translation operators. Note that these operators permit to compute efficiently $J_c(\boldsymbol{q})$, $J_\varphi(\boldsymbol{q})$ and their time derivatives $\dot{J}_c(\boldsymbol{q})$, $\dot{J}_\varphi(\boldsymbol{q})$. In particular, the Composite Rigid Body Algorithm (CRBA) (Featherstone and Orin, 2000) allows us to evaluate the inertia matrix $H(\boldsymbol{q})$ and the nonlinear terms $\boldsymbol{h}(\boldsymbol{q}, \dot{\boldsymbol{q}})$. The balancing of the robot is achieved by calculating the Jacobian of its center of gravity (Sugihara and Nakamura, 2002), which is, in our case, an inequality task to maintain the CoM within the support polygon shaped by the contacts between the feet and the ground. We derive the task Jacobian for obstacle avoidance as reported in (Faverjon and Tournassoud, 1987).

For validating the proposed scheme, we designed two scenarios in which the HRP-2 performs manipulation tasks with massless objects, while simultaneously takes advantage of its residual redundancy to maintain balance and to avoid obstacles and joint limits. In both scenarios the robot does not need to move its feet from their initial pose in order to accomplish the global task. Also, the friction coefficient between the feet and the ground is assumed to be infinite. It is important to mention that the real geometric and dynamic parameters of the HRP-2 robot are used. The current implementation uses C++ with Blas and Lapack for numerical

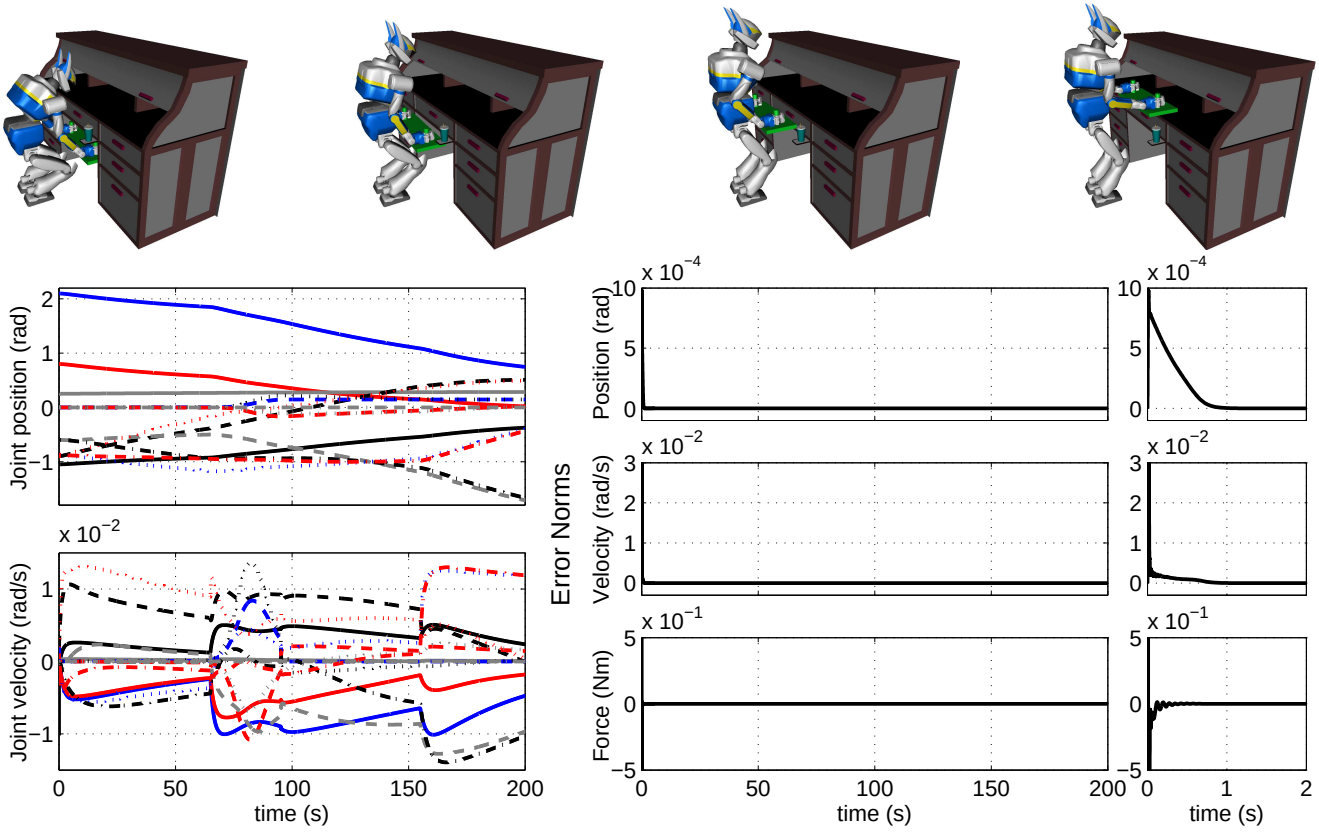

Figura 2. **Top row**: A sequence of snapshots representing the evolution of the first scenario: the HRP-2 transports a tray from underneath a desk to the top of it. **Second and third rows**: left column, the joint and velocity profiles are shown. **Last two columns**: The position, velocity and force normal errors are shown.

algebra operations and Matlab for control and visualization. Fig. 2 illustrates how the robot transports an object from an initial to a final pose, by applying the corresponding contact forces on the object surface. The object is represented as a rectangular tray with two cylindrical lugs and the global task is to displace it from underneath a desk to a space located over it, while avoiding collisions with all obstacles in the environment. We assume that the humanoid hands have already contacted the object. The hierarchical structure of tasks for this scenario considers the following mixed tasks:

Priority	Equality Task	Inequality Task
1	Poses of the feet	CoM projection
2	Poses of the hands	Avoid joint limits
3	Look at the object	Avoid obstacles

The results are shown in Fig. 2. Observe that the global task is accomplished successfully and the robot avoids the collision between the tray and the desktop. Note that the joint and velocity profiles are smooth and their values follow closely the desired profiles. In Fig. (3) the humanoid is pushing an object from one place to another by applying the corresponding contact force on the object surface. The robot exerts a predefined force on one of the lateral faces of the telephone, note that this force is normal to the contact surface. The assumptions are: the location and magnitude of the force needed to slide the object is known and the desktop surface is horizontal and therefore the gravitational force does not affect the object displacement. The hierarchical structure of tasks remains the same. The sequence of snapshots shows the evolution of the global task along the top row of Fig. (3). We observe that the humanoid is capable to move the object over the desktop while maintaining its balance. Also notice the robust tracking of the desired joint and velocities profiles.

VI. Conclusion

We proposed a motion generation and control scheme to deal with constrained humanoid motions. The controller does not need to calculate any dynamic parameter to design the generalized torque inputs to be applied to humanoids. Moreover, the residual redundancy represents a key element to design the desired joint velocity profiles based on a task-priority framework. The current formulation accounts for frictionless contact problems. Preliminary results show that our scheme can be successfully applied in practice. We are currently working on a formulation for computing multi-rigid-body dynamics with frictional contacts which is necessary to control the switches between free and constrained motions.

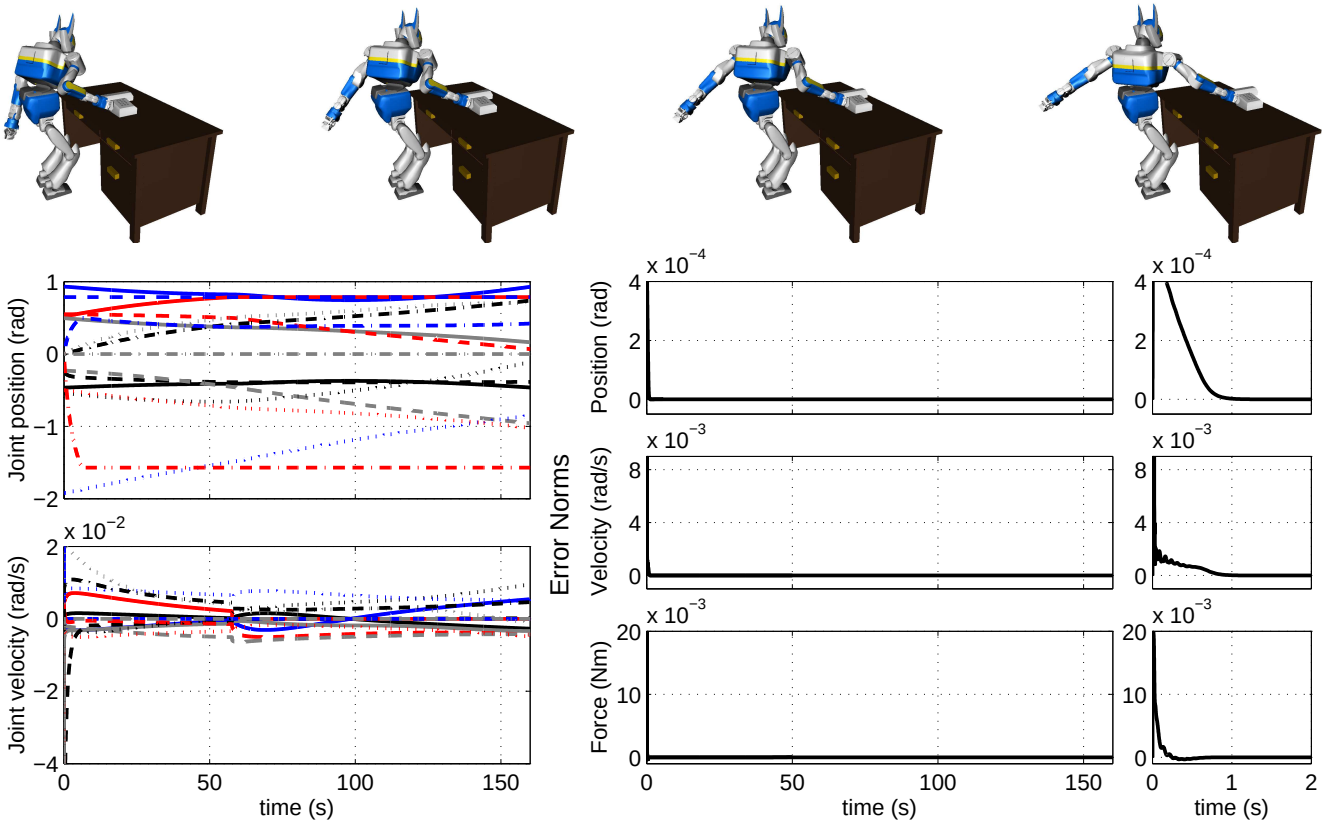

Figura 3. **First row**: A sequence of snapshots representing the solution of the second problem: the HRP-2 pushes a telephone over a desktop while avoiding joint limits and maintaining its balance. **Second and third rows**: left column, the joint and velocity profiles are shown. **Last two columns**: The position, velocity and force normal errors are shown.

VII. Acknowledgments

This work has been supported by the National Council of Science and Technology (CONACyT) projects 133346 and 84855.

References

Arechavaleta, G., A. Barrios, G. Jarquín and V. Parra-Vega (2010). Simultaneous local motion planning and control for cooperative redundant arms. In: *IEEE/RSJ Int. Conf. on Intelligent Robots and Systems*. Taipei, Taiwan. pp. 4534–4539.

Baerlocher, P. and R. Boulic (2004). An inverse kinematic architecture enforcing an arbitrary number of strict priority levels. *International Journal of Computer Graphics* **20**(6), 402–417.

Dubowsky, S. and E. Papadopoulos (1993). The kinematics, dynamics, and control of free-flying and free-floating space robotic systems. *IEEE Transaction on Robotics and Automation* **9**(5), 531–543.

Faverjon, B. and P. Tournassoud (1987). A local based approach for path planning of manipulators with a high number of degrees of freedom. In: *IEEE Int. Conf. on Robotics and Automation*. Raleigh, NC, USA. pp. 1152–1159.

Featherstone, R. and D. Orin (2000). Robot dynamics: Equations and algorithms. In: *IEEE Int. Conf. on Robotics and Automation*. San Francisco, CA, USA. pp. 826–834.

Gienger, M., H. Janssen and C. Goerick (2005). Task-oriented whole body motion for humanoid robots. In: *IEEE/RAS Int. Conf. on Humanoids Robots*. Tsukuba, Japan. pp. 238–244.

Hyon, S.-H. and G. Cheng (2006). Passivity-based full-body force control for humanoids and application to dynamic balancing and locomotion. In: *IEEE/RSJ Int. Conf. on Intelligent Robots and Systems*. Beijing, China. pp. 4915–4922.

Kanoun, O. (2011). Real-time prioritized kinematic control under inequality constraints for redundant manipulators. In: *Robotics: Science and Systems VII*. Los Angeles, CA, USA.

Kanoun, O., F. Lamiraux and P.-B. Wieber (2011). Kinematic control of redundant manipulators: Generalizing the task-priority framework to inequality task. *IEEE Transactions on Robotics* **27**(4), 785–792.

Khatib, O. (1987). A unified approach for motion and force control of robot manipulators: The operational space formulation. *IEEE Journal of Robotics and Automation* **3**(1), 43–53.

Liégeois, A. (1977). Automatic supervisory control of the configuration and behavior of multibody mechanisms. *IEEE Transactions on Systems, Man and Cybernetics* **7**(12), 868–871.

Nakamura, Y., H. Hanafusa and T. Yoshikawa (1987). Task-priority based redundancy control of robot manipulators. *International Journal of Robotics Research* **6**(2), 3–15.

Raibert, M.-H. and J. J. Craig (1981). Hybrid position/force control of manipulators. *ASME Journal of Dynamic Systems, Measurement and Control* **102**(2), 126–133.

Saab, L., N. Mansard, F. Keith, J.-Y. Fourquet and P. Soueres (2011). Generation of dynamic motion for anthropomorphic systems under prioritized equality and inequality constraints. In: *IEEE Int. Conf. on Robotics and Automation*. Shanghai, China. pp. 1091–1096.

Sentis, L., J. Park and O. Khatib (2010). Compliant control of multicontact and center-of-mass behaviors in humanoid robots. *IEEE Transactions on Robotics* **26**(3), 483–501.

Siciliano, B. and J.-J.E. Slotine (1991). A general framework for managing multiple tasks in highly redundant robotic systems. In: *IEEE Int. Conf. on Advanced Robotics*. Pisa, Italy. pp. 1211–1216.

Sugihara, T. and Y. Nakamura (2002). Whole-body cooperative balancing of humanoid robot using cog jacobian. In: *IEEE Int. Conf. on Intelligent Robots and Systems*. Lausanne. pp. 2575–2580.

Utkin, V. (1992). *Variable Structure Systems: Control and Optimization*. MIR.